RSC Advances

PAPER

View Article Online
View Journal | View Issue

Cite this: *RSC Adv.*, 2026, **16**, 29515

Study on the gasification characteristics of wool in supercritical water for hydrogen production

Wentao Deng,[a] Yun Chao,*[ab] Qian Li, *[a] Bin Chen, [b] Zhigang Liu,[bc] Huiming Chen,[bd] Lei Yi[e] and Chuanli Liu[c]

Received 12th April 2026
Accepted 26th May 2026

DOI: 10.1039/d6ra03076a

rsc.li/rsc-advances

Waste wool, a protein-based waste from textile and livestock industries, represents a promising yet underexplored feedstock for clean hydrogen production. In supercritical water, its keratin structure undergoes rapid hydrolysis and depolymerization, enabling efficient conversion into hydrogen-rich gas with minimal char formation. In this study, a systematic investigation of wool SCWG was conducted by evaluating the effects of temperature, feedstock concentration, residence time, and catalyst addition. Compared with conventional biomass feedstocks, the unique protein structure of wool leads to distinct gasification behavior and high hydrogen production potential. Higher temperature, lower feedstock concentration, and moderately long residence time significantly enhance carbon conversion and gas yield. Under optimal conditions (600 °C, 2 wt% feedstock concentration, and 5 min residence time), carbon conversion efficiency reached 95.71%, hydrogen efficiency reached 119.26%, and gas yield reached 42.72 mol kg^{-1}. Furthermore, the addition of Cu-3% Al_2O_3 catalyst significantly improves hydrogen production and gasification efficiency, highlighting the synergistic role of catalytic effects and feedstock characteristics. These findings provide new insights into the gasification behavior of protein-rich biomass and demonstrate that supercritical water gasification is a promising and efficient pathway for converting waste wool into clean hydrogen energy.

1. Introduction

As global demand for clean, efficient energy grows, hydrogen has gained popularity for its high energy density and ecological benefits.[1,2] When burned, hydrogen has a lower LHV of 142.3 MJ kg^{-1} and produces water as a byproduct, with no greenhouse gases or pollutants. For this reason, hydrogen is recognized as one of the most promising secondary energy sources.[3,4] Hydrogen is rarely elemental, and must be produced by energy conversion. The methods used to produce hydrogen directly affect the performance of hydrogen energy systems.[5] Currently, most hydrogen production worldwide relies on fossil-fuel-based processes, commonly referred to as "grey hydrogen", which primarily include steam reforming of natural gas and coal gasification.[6] These processes are mature and economically viable; however, they are associated with significant CO_2 emissions. In addition, water electrolysis is another alternative technology for hydrogen production, which can produce high-purity hydrogen but suffers from high energy consumption and strong dependence on electricity sources.[7–9] Against the backdrop of the "carbon peak and carbon neutrality" goals, there is therefore an urgent need to develop cleaner, more sustainable hydrogen production technologies to replace traditional high – carbon approaches.[10]

As the only renewable carbon-based resource, biomass is regarded as a key feedstock for green hydrogen production. Biomass gasification for hydrogen production can achieve a carbon – neutral cycle to a certain extent, but biomass has high volatile content and low energy density under conventional gasification or steam reforming conditions. It easily generates tar and coke during the conversion process, which impairs the quality of the product gas and increases the operational complexity of the system.[11–14] High-temperature steam reforming further aggravates the formation of coke and polycyclic aromatic hydrocarbons (PAHs), which severely limit hydrogen yield and reaction stability.[15,16] To reduce byproduct formation and improve hydrogen production performance, researchers have developed various catalyst systems, including alkali metals, alkaline earth metals, and nickel-based catalysts, and these systems have brought about partial improvements in hydrogen yield and tar conversion efficiency.[17–20] For example,

[a]School of Energy and Mechanical Engineering, Jiangxi University of Science and Technology, Nanchang 330013, China. E-mail: chaoyun2001_09@126.com; wuli198679@163.com
[b]State Key Laboratory of Multiphase Flow in Power Engineering (SKLMF), Xi'an Jiaotong University, Xi'an 710049, China
[c]International Institute for Innovation, Jiangxi University of Science and Technology, Nanchang 330013, China
[d]School of Mechanical and Electrical Engineering, Jiangxi University of Science and Technology, Ganzhou 341000, China
[e]Jiangxi Provincial Key Laboratory of Particle Technology, Jiangxi University of Science and Technology, Ganzhou 341000, China

Zhang *et al.*[21] used LAO and LSAO-supported nickel catalysts in toluene steam reforming, raising the hydrogen yield to 78.18%; Kuchonthara *et al.*[22] added K_2CO_3/NiO/γ-Al_2O_3 during the steam reforming of rice husk – derived tar, cutting the tar yield. from 36.2% to 28.9% while increasing the hydrogen yield from 24.1% to 33.5%; Luo *et al.*[23] added CaO to the steam gasification of pine sawdust, achieving a 2.39-fold increase in hydrogen yield and a 16% reduction in tar yield. Even so, catalytic gasification still faces challenges such as catalyst deactivation, carbon deposition, and complex reaction pathways, which means the core problem of tar formation has not been fundamentally solved.

Supercritical water, defined as water above 374.3 °C and 22.1 MPa, exhibits unique physicochemical properties such as high diffusivity, low dielectric constant, and enhanced mass transfer capability.[24,25] Supercritical water decreases the polarity of water and thus enhances solubility of organic compounds while the higher ion product promotes radical and ionic reactions.[26,27] Biomass is rapidly hydrolyzed, pyrolyzed and reformed in homogeneous state, which inhibits formation of phenolics and tar and allows efficient and clean gasification. Recently, SCWG has been applied to various biomass feedstocks such as agricultural and forest waste, food waste, sewage sludge and oily waste.[28–31] The main parameters that influence hydrogen production are reaction temperature, feed concentration, residence time, and catalyst type. Different feedstocks have different hydrogen yields under optimal conditions.[32–35] For instance: Su *et al.*[34] reported a hydrogen yield of 1.74 mol kg^{-1} from food waste at a concentration of 5 wt%, a temperature of 450 °C and a residence time of 20 min; Nanda *et al.*[36] achieved a hydrogen yield of 3.37 mol kg^{-1} from fructose at 4 wt%, 700 °C and 1 min, and fructose is a model compound for fruit and vegetable waste. In addition, catalysts, especially noble metal and nickel-based catalyst systems, can improve hydrogen yield and selectivity.[37–41] Borges *et al.*[37] found that using $NiFe_2O_4$ in the gasification of eucalyptus sawdust increased the hydrogen content by 60%, while Huang *et al.*[38] demonstrated that nickel nanoparticles can enhance the hydrogen yield from glucose gasification. Overall, SCWG has the advantages of high gasification efficiency, minimal coking, and high-quality product gas, which makes it highly suitable for processing complex biomass feedstock systems.

Notably, most fundamental studies on SCWG have been conducted in batch-type reactors, which provide a closed and well-controlled reaction environment. In such systems, the gradual heating process and relatively long effective residence time enable prolonged interaction between intermediates and supercritical water, thereby promoting secondary reactions such as steam reforming and water–gas shift. As a result, hydrogen yields in batch SCWG systems typically fall within the range of 1–5 mol kg^{-1} for carbohydrate-based feedstocks under comparable conditions, whereas significantly higher hydrogen production can be achieved for protein-rich feedstocks due to their distinct chemical composition and enhanced participation of water in hydrogen generation.[42] Therefore, batch reactors are widely regarded as an appropriate platform for investigating intrinsic reaction mechanisms and gasification behavior of complex biomass.

Wool is one of the most abundant protein-based waste materials generated from the textile and livestock industries and has attracted increasing attention due to its high keratin content.[43,44] Global annual wool production exceeds 1–2 million tons; however, less than 10% of waste wool is effectively recycled, with most being discarded or converted into low-value products.[41,45] In China, large quantities of waste wool are generated every year, while the effective recycling rate remains relatively low.[46] The accumulation and improper disposal of waste wool may lead to environmental concerns and resource waste.As a protein-rich biomass, wool keratin contains abundant peptide bonds and heteroatoms, making it a potentially valuable feedstock for hydrogen-rich gas production. Compared with conventional thermochemical processes such as pyrolysis and dry gasification, supercritical water gasification (SCWG) is more suitable for treating wet and nitrogen-containing biomass without the need for energy-intensive drying. Therefore, the utilization of waste wool through SCWG provides a promising pathway for resource recovery, clean hydrogen production, and high-value utilization of protein-based waste biomass.[47,48]

Compared with other protein-rich biomass such as sewage sludge, algae and animal residues, wool keratin exhibits a relatively homogeneous and well-defined molecular structure dominated by keratin, with abundant disulfide bonds and stable peptide linkages. In contrast, sewage sludge often contains high ash content and inorganic impurities that may inhibit catalytic performance, while microalgae typically present highly variable compositions and moisture content, leading to less stable gasification behavior.[49,50] These differences suggest that wool may follow distinct reaction pathways during SCWG, particularly in terms of sulfur evolution, intermediate formation, and hydrogen production mechanisms. However, systematic studies on wool SCWG focusing on hydrogen production, product distribution and catalytic effects are still lacking.

This paper uses waste wool as the feedstock to study the hydrogen production behavior by SCWG. By monitoring gaseous and liquid products simultaneously, we evaluate gasification performance in terms of CE, HE, hydrogen selectivity, gas lower heating value (LHV), molar fractions of gas components and gas yield. Carbon and hydrogen conversion pathways are investigated along with the reaction mechanism. Unlike conventional studies that primarily focus on process optimization, this work emphasizes the intrinsic relationship between protein structure and gasification behavior, and the theoretical and experimental results are presented to support clean hydrogen production from proteinbased biomass and high value resource utilization of waste wool.

1.1. Materials

The wool used here is composed mostly of keratin and contains a few elements, including moisture, lipids, and inorganic salts. Keratin is the largest component of the wool, accounting for 80–95% of the mass, while moisture is 10–17%. Lipids and inorganic salts each make 0.5–2% of the sample. The wool was collected in Xingtai, Hebei Province, shredded, and stored in

Table 1 Proximate and ultimate analyses of wool samples

Ultimate analysis (wt%)				
C	H	N	O	S
42.93	6.2175	14.305	28.5415	2.586
Industrial Analysis(wt%)				
Moisture	Ash content	Volatile component	Fixed carbon	Total
9.805	0.355	76.6	13.24	100

a sealed desiccator for subsequent experiments. Ultimate and closest estimates of the wool are summarized in Table 1. The lower heating value (LHV) of wool was calculated to be approximately 17.17 MJ kg^{-1}.

1.2. Experimental apparatus

We used quartz tubes as experimental containers due to their small size, rapid heating, and transparency. The tubes had an inner diameter of 2.08 mm, an outer diameter of 5 mm, and a length of 200 mm. Fig. 1 shows the schematic of the micro quartz tube reactor, which consists mainly of a temperature controller, heating wire, thermocouple, and pull rod. The reactor is designed for operation at 1000 °C (with a monitoring accuracy of ±0.1 °C) and can withstand a maximum internal pressure of 40 MPa (with a monitoring accuracy of ±0.1 MPa). Using quartz tubes helps to prevent side reactions caused by slow heating. All experiments were performed using a high-temperature and high-pressure resistant reactor system. Temperature and pressure were continuously monitored during operation to ensure safe and stable experimental conditions under supercritical water environments.

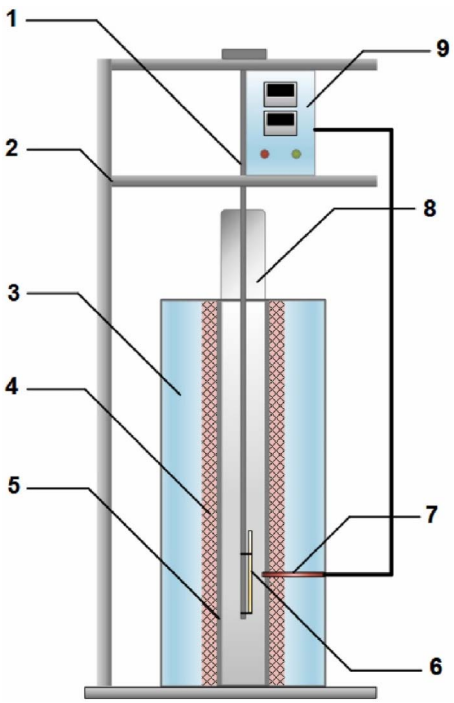

Fig. 1 Schematic diagram of the quartz tube reactor system. (1 sliding rod; 2 support frame; 3 insulation layer; 4 heating filament; 5 internal cylinder; 6 quartz tube; 7 thermocouple; 8 insulation cover; 9 temperature controller).

1.3. Experimental procedure

Before SCWG experiments, wool samples were weighed (0.01 mg precision, analytical balance), placed on the quartz tube bottom, ultrapure water was injected *via* a 10 μL micro syringe for mixing, nitrogen purging to remove the internal air, tube opening was sealed with an oxy-hydrogen flame to ensure bubble- and crack-free sealing.

During the experiment, the quartz tubes in the reactor will gradually be heated to the set temperature. At this point, the timing begins. After reaching the specified residence time, the quartz tubes will be removed and allowed to cool down. After cooling is complete, the products will be collected. The gas products will be collected in a stainless steel tube. The specific collection method is as follows: first, blow high-purity nitrogen gas through the stainless steel tube to expel the internal air. Then, place the quartz tube inside and seal it with a rubber stopper. Next, use another steel tube to strike forcefully, causing the quartz tube to break. The gas was collected in the steel tube, and then connect one end of a rubber tube to the exhaust valve of the steel tube and the other end to a U-shaped tube with a scale. Open the exhaust valve and observe that the liquid level in the U-shaped tube drops. The difference between the liquid levels before and after is the volume of the produced gas. The liquid products were collected in test tubes, and the specific collection method is as follows: first, vigorously shake the quartz tube to cause the liquid to accumulate at the other end. Then, use a glass knife to make a circular cut at an appropriate position in the quartz tube, and then break the quartz tube by hand, collecting the liquid product in the test tube. All experiments were performed in triplicate, and gas composition measurements were repeated to ensure data reliability and reproducibility.

1.4. Analytical methods

1.4.1. Analysis of gaseous products. The analysis of gaseous products is carried out using an Agilent 8890 gas chromatograph, equipped with a thermal conductivity detector. The temperatures of the chromatographic column, the injection port, and the thermal conductivity detector are set at 250 °C. The carrier gas is high-purity argon (99.99%), with a flow rate of 30 ml min^{-1}. Prior to sample analysis, the GC system was calibrated using standard gas mixtures containing H_2, CO, CO_2, CH_4, C_2H_4, C_2H_6, and N_2. Quantification of gaseous products was performed based on calibration curves obtained from the peak areas of the standard gases. Repeated measurements were conducted to ensure analytical reliability.

1.4.2. Analysis of liquid-phase products. First, add an equal amount of ethyl acetate to the liquid phase product collected in the test tube. Then, centrifuge the mixture. After centrifugation, use a micropipette to collect the upper layer of the extracted

liquid. Inject this upper layer into the Agilent 7000D gas chromatography-mass spectrometer (GC-MS) manually. Set the column chamber to 60 °C as the starting temperature. Heat the chamber to 95 °C at 35 °C per minute and hold for 5 minutes. Then, raise the temperature to 120 °C and hold for 6 minutes. Subsequently, increase the temperature to 200 °C, hold for 3 minutes, and finally raise it to 250 °C, holding for 4 minutes. Start the detection by pressing the start button on the GC-MS.

1.5. Gas production performance indicators

To assess the conversion behavior of wool during the gasification process, multiple quantitative parameters were adopted to characterize system performance. These parameters comprise CE, HE, hydrogen selectivity, LHV, molar distribution of gaseous components, and overall gas yield. The detailed mathematical expressions used for their determination are presented below:

$$\mathrm{CE}(\%) = \frac{m_{\mathrm{C,gas}}}{m_{\mathrm{C,feedstock}}} \times 100\%$$

$$\mathrm{HE}(\%) = \frac{m_{\mathrm{H,gas}}}{m_{\mathrm{H,feedstock}}} \times 100\%$$

$$\mathrm{H_2selectivity}(\%) = \frac{Y_{\mathrm{H_2}}}{Y_{\mathrm{CO}} + Y_{\mathrm{CH_4}} + Y_{\mathrm{CO_2}} + Y_{\mathrm{C_2H_6}} + Y_{\mathrm{C_2H_4}}} \times 100\%$$

$$\mathrm{LHV}\left(\mathrm{MJ\ Nm^3}\right) = \frac{107.98 \times Y_{\mathrm{H_2}} + 126.36 \times Y_{\mathrm{CO}} + 358.18 \times Y_{\mathrm{CH_4}}}{1000}$$

$$\mathrm{Gas\ yield}\left(\mathrm{mol\ kg^{-1}}\right) = \frac{\text{The mol number of gaseous product}}{\text{The mass of feedstock}}$$

$$\text{Gas molar fraction} = \frac{\text{The mol number of gaseous product}}{\text{The mol number of all the gaseous products}} \times 100\%$$

In the equations, $m_{\mathrm{C,gas}}$ stands for total mass of carbon in.gaseous product, $m_{\mathrm{C,feedstock}}$ stands for total mass of carbon in feedstock, $m_{\mathrm{H,gas}}$ stands for total mass of hydrogen in gaseous product, $m_{\mathrm{H,feedstock}}$ stands for total mass of hydrogen in feedstock. LHV stands for the low heat value of gas. $Y_{\mathrm{H_2}}$, $Y_{\mathrm{CO_2}}$, $Y_{\mathrm{CH_2}}$, Y_{CO}, $Y_{\mathrm{C_2H_2}}$ and $Y_{\mathrm{C_2H_2}}$ represent the gas yield of component H_2, CO_2, CH_4, CO, C_2H_4 and C_2H_6, respectively.

2. Results and discussion

2.1. Wool gasification characteristics

This section discusses wool gasification characteristics under varying conditions: reaction temperature (°C), feedstock concentration (wt%), and residence time (min). For context, the primary reactions in supercritical water gasification of organic matter include steam reforming, water–gas shift, and methanation.[51,52]

$$\text{Steam reforming: } \mathrm{C + H_2O \rightarrow CO + H_2}\ \Delta H_{298\mathrm{K}} = 131.29\ \mathrm{KJ\ mol^{-1}}$$

$$\text{Water–gas shift: } \mathrm{CO + H_2O \leftrightarrow CO_2 + H_2}\ \Delta H_{298\mathrm{K}} = 41.17\ \mathrm{KJ\ mol^{-1}}$$

$$\text{Methanation: } \mathrm{CO + 3H_2 \leftrightarrow CH_4 + H_2O}\ \Delta H_{298\mathrm{K}} = -206.10\ \mathrm{KJ\ mol^{-1}}$$

$$\mathrm{CO + 4H_2 \leftrightarrow CH_4 + 2H_2O}\ \Delta H_{298\mathrm{K}} = -164.93\ \mathrm{KJ\ mol^{-1}}$$

2.1.1. Effect of reaction temperature. We investigated the effect of reaction temperature on wool SCWG at 2 wt% feedstock and 5 min residence time with reaction temperatures at 400 °C, 450 °C, 500 °C, 550 °C, and 600 °C (50 °C interval). Fig. 2(a) shows the different effects of reaction temperature on CE and HE in the test conditions (5 min residence time, 9 wt%). CE increases by 48.25% to 95.71% with temperature increase of 400 °C to 600 °C, indicating more wool organic carbon is converted to gas phases at higher temperature. In addition, HE is up by 43.53% to 119.26%. In the low temperature range (400–450 °C), CE and HE remain relatively low. This is due to the stability of wool proteins, where intramolecular peptide and disulfide bonds are incompletely fractured. Thermal cracking dominates the reaction system, and water-involved reforming and water–gas shift reactions restrict carbon and hydrogen to the gas phase. At 500 °C CE and HE show distinct growth, suggesting that high temperatures facilitate deep cracking of keratin macromolecules while further reforming intermediate oxygenated organics, tar, and solid residual carbon. Temperature increases to 550–600 °C, the CE approaches 100%, confirm near-complete conversion of wool carbon to gas-phase products with significant reductions in coking and refractory solids. This is due to increased water dissociation and diffusion in the high-temperature supercritical environment, which intensifies steam reforming and water–gas shift reactions. At low temperature, the carbon conversion efficiency curve is higher than the hydrogen production efficiency curve, and the two curves intersect around 500–550 °C. Above 500 °C, HE is above CE. This is because the release of carbon and hydrogen during SCWG depends on different pathways of the kinetic and thermodynamic, respectively. At low temperature, the pyrolysis and primary cracking of large organic molecules kickstart their decomposition, leading to rapid progress of carbon conversion reactions. At low temperatures, only a few active sites are needed for hydrolysis and reforming reactions. At the temperature above 500 °C, steam reforming and water–gas shift reactions increase much more intensely, and both the decomposition of organic intermediates and direct dissociation of water molecules produce large amounts of hydrogen. Water is highly reactive in a supercritical environment, allowing the

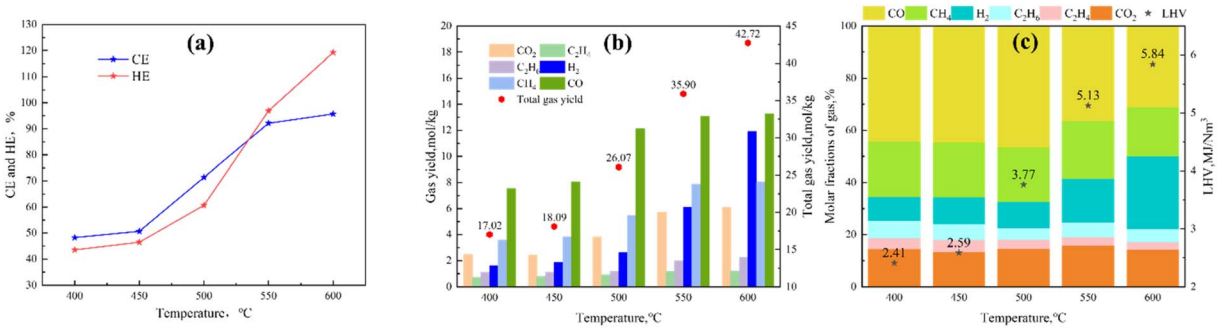

Fig. 2 Influence of reaction temperature on the supercritical water gasification of wool at a feedstock concentration of 2 wt% and a residence time of 5 min: (a) CE and HE; (b) gas yields and total gas yield; (c) molar fractions of gas and LHV.

hydrogen production to exceed the hydrogen content of the feedstock, pushing the HE value above 100%, and the CE reaches saturation. To further verify this phenomenon, a hydrogen balance analysis was conducted. The hydrogen balance based on gaseous products was approximately 119%, indicating that additional hydrogen was generated from water *via* reactions such as water–gas shift and steam reforming. A carbon balance analysis was performed under a representative condition, and the carbon balance closure was approximately 94%, indicating that most of the carbon was accounted for in the gaseous products. The apparent gas yield relative to the feedstock was estimated to be around 90%. It should be noted that this does not represent a complete mass balance of the system, as liquid-phase products and dissolved intermediates were not fully quantified.

Fig. 2(b) shows the temperature dependence of gas products in gasification. Gas products consist mostly of H_2, CO_2, CO, CH_4, C_2H_4, and C_2H_6. As the reaction temperature increases, the gas production increases to 42.72mol kg^{-1} at 600 °C compared to 17.02 mol kg^{-1} at 400 °C. High temperature favours gas formation. Major gas species form at higher temperatures. H_2 and CO_2 yields increase significantly from 1.59 and 2.46 mol kg^{-1} at 400 °C to 11.91 and 6.09 mol kg^{-1} at 600 °C, respectively. Notably, the yield of CO exhibits a pronounced increase between 450 °C and 500 °C, rising from approximately 8.04 mol kg^{-1} to 12.11 mol kg^{-1}. This behavior arises from thermal cracking and decarboxylation of oxygenated intermediates (carboxylic acids, aldehydes, ketones) generated during initial wool keratin decomposition. The effect is reflected in an increased extent of cracking and decarboxylation of these intermediates (*e.g.*, from 8.04 mol kg^{-1} to 12.11 mol kg^{-1}). At the relevant temperatures, the intermediates acquire sufficient energy to overcome activation barriers for C–O and C–C bond cleavage, which leads to release of carbon monoxide. In addition, partial oxidation reactions and the limited extent of the water–gas shift (WGS) reaction at moderate supercritical temperature favour CO accumulation. As a result, the conversion of CO to CO_2 is not complete under these conditions, leading to relatively higher CO yields. This imbalance between CO formation and its subsequent conversion contributes to the observed CO-dominant behavior in the gas products. In turn, the 450–500 °C interval is the critical time when secondary decomposition pathways are significantly accelerated. The increase in H_2 yield above 500 °C can be attributed to the combined effects of primary decomposition and secondary gasification reactions. At elevated temperatures, the thermal cracking of wool keratin is significantly intensified, leading to the continuous formation of intermediate gaseous species such as CO, CH_4, and light hydrocarbons. Meanwhile, steam reforming and water–gas shift reactions are also enhanced under supercritical conditions, contributing to additional hydrogen production. However, the simultaneous increase in CO and CH_4 yields suggests that the formation rates of these intermediates exceed their consumption rates *via* secondary reactions. Therefore, the observed increase in H_2 is not solely due to the consumption of CO and CH_4, but rather results from a dynamic balance between rapid generation of intermediates and their partial conversion into hydrogen. Similar behavior has been reported in SCWG of other biomass feedstocks, where parallel reaction pathways dominate at high temperatures.

Fig. 2(c) shows the distribution of the fractions and lower heating value of product gases at different temperatures. Reaction temperature changes the composition of gas and energy quality: if temperature increase from 400 °C to 600 °C, gas composition shifts dramatically from a temperature increase from 2.41 to 5.84 MJ Nm^{-3} (significantly up). H_2 fraction changes with temperature (9.35% increase from 400 °C to 27.87% increase from 600 °C), CO and CH_4 fractions decrease (44.30% decrease from 31.01% and 21.08% increase to 18.84%, respectively). C_2H_6 and C_2H_4 fractions decrease with temperature increase. At 400 °C, product gas is predominant by CO_2 and CH_4, low H_2 and CO fractions, which results in LHV of only 2.41–2.59 MJ Nm^{-3}, suggesting wool first thermal cracking with limited water reforming, leading to low combustible gas proportions and low energy density. As the temperature reached 500 °C, H_2 and CO fractions increased significantly, LHV reaching 3.77 MJ Nm^{-3}, reflecting the increase of steam reforming and water–gas shift reactions in supercritical water, which further convert wool-cracking intermediates (oxygenated organics, tar and light hydrocarbons) into small molecules combustible gases, improving gas energy quality. At 550–600 °C, H_2 and CO became the main gas components (with significant increases), while CH_4 and other light hydrocarbons were stable or decreased. LHV reached 5.13–5.84 MJ Nm^{-3}, suggesting that

high temperatures favor hydrogen-rich high-energy-density syngas production due to water reactivity at high temperatures which promote deep reforming of tar and solid carbon and inhibiting methanation, shifting reaction system toward H_2 and CO production.

2.1.2. Effect of feedstock concentration. Supercritical water gasification experiments were carried out using wool feedstock at concentrations of 2, 5, 7, 9, and 11 wt% while maintaining a reaction temperature of 600 °C and a residence time of 5 min. The corresponding variations in carbon conversion efficiency (CE) and hydrogen conversion efficiencyt (HE) are presented in Fig. 3(a). Overall, increasing feedstock concentration leads to a decline in both CE and HE; however, a slight recovery is observed at higher concentrations (9–11 wt%), resulting in a non-monotonic trend. At a concentration of 2 wt%, the CE and HE reached 95.71% and 119.26%, respectively. Under the same temperature and residence time conditions, increasing the feedstock concentration to 9 wt% led to decreases of 62.61% and 79.36% in CE and HE, respectively. When the concentration was further increased to 11 wt%, both indicators showed a slight recovery, with CE and HE increasing by 27.84% and 40.05%, respectively, relative to their minimum values. At relatively low feedstock concentrations, the higher water-to-organic matter ratio may provide more favorable conditions for water-mediated reactions under supercritical conditions, which could contribute to higher carbon and hydrogen conversion efficiencies. In addition, the relatively abundant aqueous phase may facilitate mass transfer and intermediate conversion during gasification. As the feedstock concentration increased, the relative water availability decreased, which may suppress reactions associated with steam reforming and intermediate conversion, thereby reducing CE and HE. Under these conditions, some intermediates may not be fully converted into gaseous products and could instead participate in competing side reactions. However, when the feedstock concentration further increased from 9 to 11 wt%, the decreasing trend of CE and HE was no longer strictly maintained. This behavior may be related to the increasingly complex reaction environment under relatively high organic loading. At elevated concentrations, the formation and interaction of keratin-derived intermediates may become more significant and could influence subsequent gasification pathways and product distribution. Previous studies have also suggested that feedstock concentration and intermediate interactions under supercritical water conditions can affect reaction behavior and gaseous product formation.[51,53] Therefore, the slight rebound in CE and HE at 11 wt% may be associated with the combined effects of intermediate formation and secondary conversion processes under high-concentration conditions.

As shown in Fig. 3(b), feedstock concentration affects individual gas component yields in wool SCWG. H_2 yield drops from 11.91 mol kg^{-1} at 2 wt% to 1.16 mol kg^{-1} at 9 wt%. The drop is particularly steep between 2 wt% and 5 wt%. CO and CO_2 yield drop from 13.25 mol kg^{-1} and 6.09 mol kg^{-1} to 3.35 mol kg^{-1} and 2.07 mol kg^{-1}, respectively. This drastic decrease in H_2 and CO_2 yields is mainly attributed to the reduced water-to-carbon ratio at higher feedstock concentrations. At low concentrations (2–5 wt%), excess supercritical water promotes steam reforming and water–gas shift reactions, enabling efficient conversion of keratin-derived intermediates into gaseous products. However, as the concentration increases, the relative water availability decreases, limiting these water-mediated reactions. As a result, intermediate products are not fully converted and may instead undergo condensation, polymerization, or char formation, thereby suppressing the formation of gaseous species such as H_2, CO, and CO_2. Therefore, the limited water availability also suppresses the formation of CO, leading to its decreasing trend with increasing feedstock concentration. However, at the highest concentration (11 wt%), a slight increase in CO yield is observed. This may be attributed to enhanced thermal cracking under high organic loading, which promotes the formation of CO from intermediate species, partially offsetting the limitation imposed by reduced water availability. As shown in Fig. 3(c), the H_2 fraction of the product gas generally decreases with increasing feedstock concentration from 2 wt% to 9 wt%, due to the reduced water-to-carbon ratio that limits steam reforming and water–gas shift reactions. However, when the concentration further increases to 11 wt%, this trend is no longer strictly followed. This deviation may be attributed to enhanced thermal cracking and secondary reactions at high organic loading, which promote the formation of gaseous products and partially offset the limitation of water availability. Gas lower heating value (LHV) is decreasing, then increasing. At low concentrations, large water participation

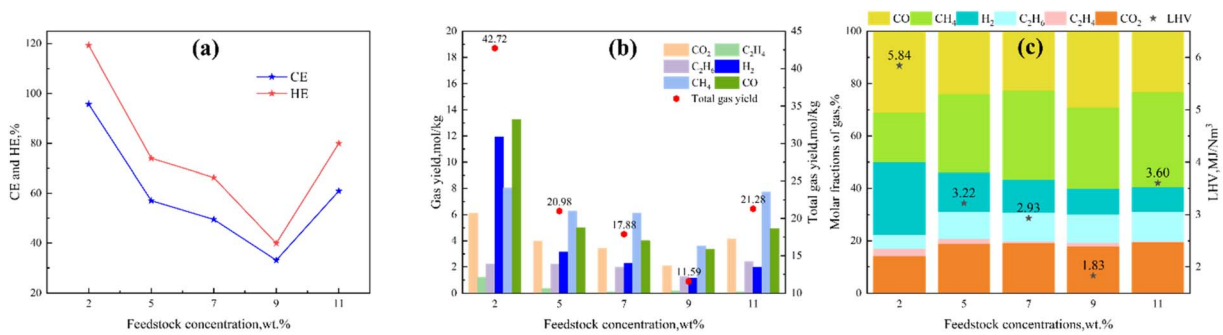

Fig. 3 Effect of feedstock concentration on the gasification behavior of wool under supercritical water conditions at 600 °C for 5 min: (a) CE and HE; (b) gas yields and total gas yield; (c) molar fractions of gas and LHV.

favors steam reforming and water–gas shift reactions, promoting H_2. As concentration increases, the effective water-to-carbon ratio decreases, making organic intermediates more susceptible to methanation and condensation, thus increasing CH_4 and reducing H_2 fraction. The largest decline in H_2 fraction occurs between 2 and 5 wt% feedstock concentrations (from 27.87% to approximately 14.94%), while the decrease is more moderate at higher concentrations (for example, from 5 wt% to 11 wt%). This pattern indicates a critical threshold in the hydrodynamics and reaction chemistry: at 2 wt% the water-to-carbon ratio is sufficient to sustain near-complete steam reforming and water–gas shift activity, maximizing H_2 selectivity. At higher feedstock loadings, the greater CH_4 mass fraction compensates for reduced H_2 production and contributes to the observed rebound in gas LHV.

2.1.3. Effect of residence time. In order to investigate the influence of residence time on the gasification characteristics of wool, experiments for gasification were conducted under the reaction conditions of 600 °C and 9 wt% with residence times of 1, 3, 5, 7, and 9 minutes, respectively. The corresponding carbon conversion efficiency (CE) and hydrogen conversion efficiency (HE) are illustrated in Fig. 4(a). Both CE and HE exhibit a non-monotonic trend, increasing with residence time and then slightly decreasing at longer residence time. As the residence time is extended from 1 min to 7 min, CE and HE increase strongly. CE increases from 34.54% to 79.66%, and HE increases from 39.43% to 101.17%, indicating that prolonging the reaction time promotes deeper hydrolysis and thermal cracking of wool keratin and completes the decomposition of complex macromolecular structures. The most significant increase of CE and HE is between 5 min to 7 min, CE increases about 41 percent, and HE about 53 percent, because we obtained optimal kinetic conditions, as at 5 min, the initial rapid cracking of wool has produced large quantities of intermediate compounds (amino acids, peptides, and oxygenated organic compounds), but they have not yet fully responded to gaseous products. At 7 min intermediates can undergo second reactions like steam reforming, water–gas shift, gasification to CO, CO_2, H_2, CH_4 and other combustible gases. High temperature (600 °C) ensures a high reaction rate, and a supercritical water environment facilitates mass transfer and diffusion, allowing efficient contact between organic fragments and reactive water species. Therefore, the period between 5–7 min is the window when the system transitions from primary decomposition to advanced reforming, and carbon and hydrogen utilization dramatically increase. The decrease was seen at 9 min. This suggests that too long residence time can trigger side reactions, such as secondary polymerization of volatile intermediates into secondary char or gaseous products from reverse reactions. Overall, the non-monotonic variation of CE and HE with residence time reflects the balance between enhanced gasification reactions at moderate residence times and the occurrence of side reactions at prolonged residence time.

Fig. 4(b) shows the distribution of gaseous products (H_2, CO_2, CH_4, CO, and light hydrocarbons C_2H_6 and C_2H_4) under different residence times. Total gas yield increased from 11.88 mol kg^{-1} to 27.87 mol kg^{-1} when residence time was extended to 7 min, and then decreased significantly to 21.08 mol kg^{-1} at 9 min. This suggests that 7 min is sufficient for complete wool gasification, while longer residence time accelerates the loss of reaction intermediates and triggers competitive side reactions. Gas production characteristics show that CH_4 and CO dominate the product gas. Yields of H_2 and CO_2 were increased continuously in the first 7 min. C_2H_4 was only at trace levels at 1 min, while C_2H_6 was suppressed in the reaction. The sharp increase in CH_4 and CO_2 yields occurs between 5 min and 7 min, the period of maximum gas production. This is due to the completion of primary thermal cracking and intensive secondary reforming reaction. By 5 min, most of the keratin macromolecules have been decomposed into oxygenated organic intermediates (carbon acids, aldehydes, ketones, tar-like substances) through hydrolysis and pyrolysis. These intermediates are not fully converted into gaseous products yet. Extending the residence time to 7 min provides enough time for these reactive species to undergo further transformation *via* steam reforming, water–gas shift, and gasification reactions in a supercritical water environment.

Fig. 4(c) shows the variation of gas fractions and lower heating value as a function of residence time. As residence time increased from 1 to 7 min, CO_2 and H_2 fractions increased to different degrees while the CO proportion decreased. At 1 min, CO, CO_2, and H_2 fractions were 34.26%, 14.26%, and 8.98%, respectively. Gas composition reached quasi-equilibrium after 7 min, CO and CO_2 stabilizing at 22.37% and 22.07%,

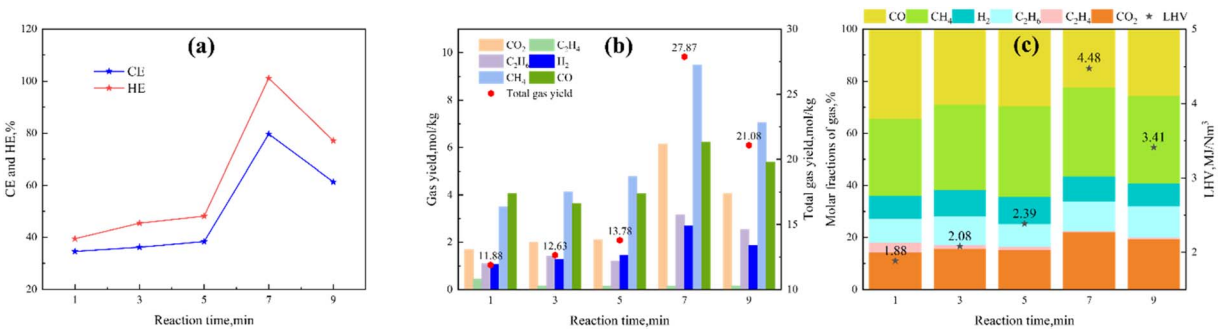

Fig. 4 Effect of residence time on the gasification behavior of wool under supercritical water conditions at 600 °C and 9 wt% feedstock concentration: (a) CE and HE; (b) gas yields and total gas yield; (c) molar fractions of gas and LHV.

respectively, H_2 reached 10.46% at 5 min. Energy density increased significantly after 5 min to a maximum of 4.48 MJ Nm^{-3} at 7 min. In the first reaction phase, oxygen groups in wool cracking with decarboxylation and carbonyl cleavage reactions produced rapid CO and CO_2 production; however incomplete water–gas shift reaction produced high CO molar fractions. As the residence time extended to 5–7 min, CO was consumed by water–gas shift reaction and converted into H_2 and CO_2 with reduced CO content and continuous H_2 increase. This improved gas system reducibility and energy density, leading to maximum LHV at 7 min.

2.2. Influence of catalyst selection and loading amount on gasification performance

Catalytic gasification tests were carried out at 600 °C using a wool feedstock concentration of 9 wt% and a residence time of 5 min, with the catalyst-to-feedstock mass ratio fixed at 1 : 1. Copper-containing catalysts are generally considered to facilitate the decomposition of large organic structures, while Al_2O_3 may contribute to improved dispersion and structural stability.[54–56] Based on these considerations, Cu and Cu–Al_2O_3 composite catalysts were employed in this work.

The corresponding hydrogen conversion efficiency (HE), carbon conversion efficiency (CE), and hydrogen selectivity obtained with Cu, Cu-3% Al_2O_3, and Cu-7% Al_2O_3 are summarized in Fig. 5(a), with the non-catalytic case serving as the reference. Compared with the non-catalytic run, the addition of Cu slightly increased hydrogen selectivity, while the carbon conversion efficiency (CE) remained nearly unchanged and the hydrogen efficiency (HE) showed a slight decrease. The addition of Cu-3% Al_2O_3 increased wool CE and HE from 38.32% and 48.17% to 77.95% and 99.23%, respectively, but with lower hydrogen selectivity. Cu-7% Al_2O_3 led to decreases in CE, HE, and hydrogen selectivity. These results suggest that different Cu-based catalysts may influence the reaction pathways during wool SCWG.

Cu species may facilitate reactions such as CO hydrogenation and water–gas shift, thereby contributing to enhanced hydrogen selectivity. However, their ability to promote deep cracking of macromolecular organic structures and aromatic intermediates may be limited, which could explain the relatively small improvement in CE and HE observed with Cu alone. The presence of Al_2O_3 in Cu-3% Al_2O_3 may contribute to increased surface area and provide sites that could facilitate chain scission, reforming, and gasification of keratin-derived intermediates, leading to improved carbon and hydrogen conversion efficiencies. However, enhanced cracking and reforming may also increase the formation of CO and CO_2, thereby reducing hydrogen selectivity. When the Al_2O_3 content is further increased to 7%, the proportion of non-selective reactions may increase, which could explain the observed decrease in hydrogen selectivity. These observations suggest that the metal-support ratio in the Cu–Al_2O_3 system may play an important role in determining the gasification performance.[53–55]

Fig. 5(b) shows individual component gas yields and total gas yields under different catalysts. Cu addition slightly lowered the total gas yield compared to the non-catalytic control, whereas Cu-3% Al_2O_3 and Cu-7% Al_2O_3 increased total gas yield. All three catalysts slightly increased H_2 yields and influenced gas-phase reactions. Cu species may promote hydrogenation or equilibrium conversion of specific CO/CO_2 species, thereby adjusting gas composition with limited impact on total gas production. In contrast, Cu–Al_2O_3 composite catalysts may enhance overall gas formation due to the combined effects of Cu species and the Al_2O_3 support. Al_2O_3 may act as a thermally stable support and could help maintain the dispersion of Cu-containing species under supercritical conditions.[53–55] In addition, its surface properties may facilitate interactions with intermediates and water, which could contribute to enhanced gasification reactions. As a result, increases in CH_4, CO, and CO_2 yields are observed with composite catalysts, suggesting a shift toward more extensive gasification pathways.

Fig. 5(c) presents the gas mole fractions and LHV under different catalysts. The gas composition and LHV vary significantly with catalyst type. The Cu-only catalyst increases the H_2 molar fraction while slightly reducing LHV. This behavior may be associated with reactions such as water–gas shift, which increase H_2 production but may suppress the formation of higher-heating-value hydrocarbons such as CH_4 and C_2H_6. In contrast, Cu–Al_2O_3 composite catalysts may exhibit dual catalytic functions, where Cu species contribute to reforming and water–gas shift reactions, and the Al_2O_3 support may influence the adsorption and transformation of organic intermediates.

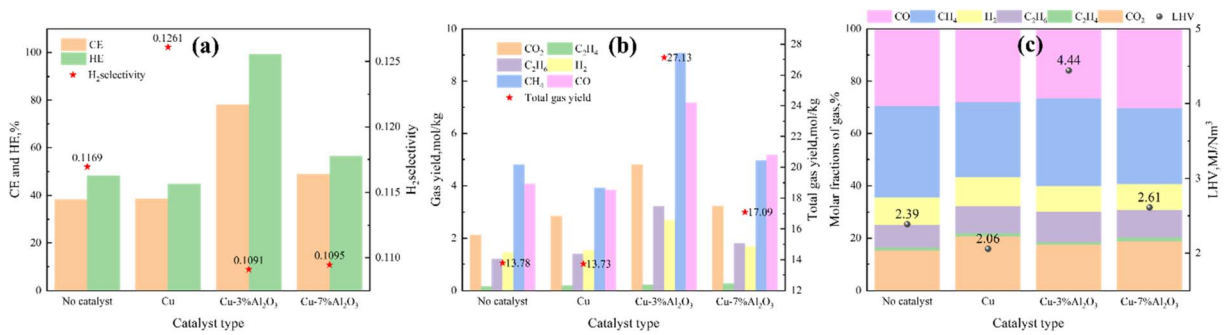

Fig. 5 Influence of catalyst type on the supercritical water gasification behavior of wool at 600 °C with a residence time of 5 min and a feedstock concentration of 9 wt%: (a) CE, HE, and hydrogen selectivity; (b) gas yields and total gas yield; (c) molar fractions of gas and LHV.

Table 2 Catalyst loading of Cu-3%Al_2O_3 and corresponding wool mass

Cu-3% Al_2O_3 loading ratio	Cu-3% Al_2O_3 mass/mg	Wool mass/mg
0.5	4.5	9
1	9	9
1.5	13.5	9

This combined effect could promote the formation of light hydrocarbons and improve LHV.

Preliminary experiments showed that Cu-3% Al_2O_3 promotes wool SCWG; therefore, its loading effect was further investigated at 600 °C, 9 wt% feedstock concentration, and 5 min residence time. The specific catalytic masses are shown in Table 2.

Fig. 6(a) presents CE, HE, and hydrogen selectivity under different catalyst loadings. The catalyst loading is defined as the mass ratio of catalyst to biomass (wool), excluding water. Compared to the non-catalytic control, all loadings improved CE and HE, whereas hydrogen selectivity increased only at the highest loading. At a catalyst loading of 1, CE and HE reached their maximum values of 77.95% and 99.29%, respectively, while hydrogen selectivity slightly decreased. This improvement may be associated with a more favorable distribution of active sites, which could enhance the interaction between catalyst surfaces and reactive intermediates without significant mass transfer limitations. At moderate loading, catalytic sites may be sufficient to promote hydrolysis, reforming, and water–gas shift reactions, enabling efficient conversion of organic carbon and hydrogen into gaseous products.[53,55]

At higher loading (1.5), CE and HE decreased, while hydrogen selectivity increased. This behavior may be related to possible particle aggregation or mass transfer limitations, which could reduce the accessibility of active sites and hinder the conversion of intermediates. As a result, fewer secondary reactions may occur, allowing a larger fraction of hydrogen to remain as H_2, thereby increasing selectivity.

Fig. 6(b) shows gas yields under different Cu-3% Al_2O_3 loadings. All loadings increased total gas yield, with the highest value observed at loading 1. This may be attributed to a balance between active site availability, dispersion, and mass transfer. At lower loading, limited catalytic sites may restrict gasification, whereas at higher loading, possible aggregation and diffusion limitations may reduce catalytic efficiency.[53–55]

As shown in Fig. 6(c), catalyst loading of 1 yields the highest CH_4 molar fraction and favorable gas composition for improved LHV. The higher CH_4 yield may be associated with enhanced methanation-related reactions, possibly facilitated by the availability of H_2 and CO/CO_2 intermediates. Meanwhile, the Al_2O_3 support may influence the transformation of oxygenated intermediates, contributing to the formation of CO, CO_2, and light hydrocarbons.

2.3. Mechanism study of wool gasification in supercritical water

Table 3 presents the distribution and relative proportions of organic compounds in the liquid-phase products obtained from wool SCWG at varying residence times. GC-MS analysis suggests the liquid-phase transformation behavior of wool under supercritical water conditions. At 1 min, the liquid products mainly contain pyrrole and toluene, with peak areas reaching 100% (pyrrole) and 85% (toluene). This may indicate rapid cleavage of keratin peptide bonds, accompanied by possible cyclization of nitrogen-containing amino acids and conversion of aromatic amino acids into alkylbenzenes. At 3 min, pyrrole remains abundant, while the content of toluene decreases with the appearance of trace unsaturated and cyclic hydrocarbons. This could suggest continuous side-chain cleavage and possible molecular rearrangement processes. At 5 min, ethylbenzene (8.0%) and phenol are detected, while pyrrole content decreases. This may imply that aromatic intermediates undergo further transformation, possibly through alkyl rearrangement, dehydrogenation, and partial oxidation reactions. At 7 min, phenol and polycyclic aromatic hydrocarbons (PAHs, such as naphthalene) are observed, which may be associated with further dehydrogenation and condensation of monocyclic aromatic intermediates. At 9 min, the peak area of phenol increases significantly (7.1%), while pyrrole and toluene remain at relatively high levels. This may suggest the coexistence of relatively stable heterocyclic compounds and newly formed oxygenated aromatic compounds. The formation of *m*-aminophenylacetylene at longer residence time may indicate deeper

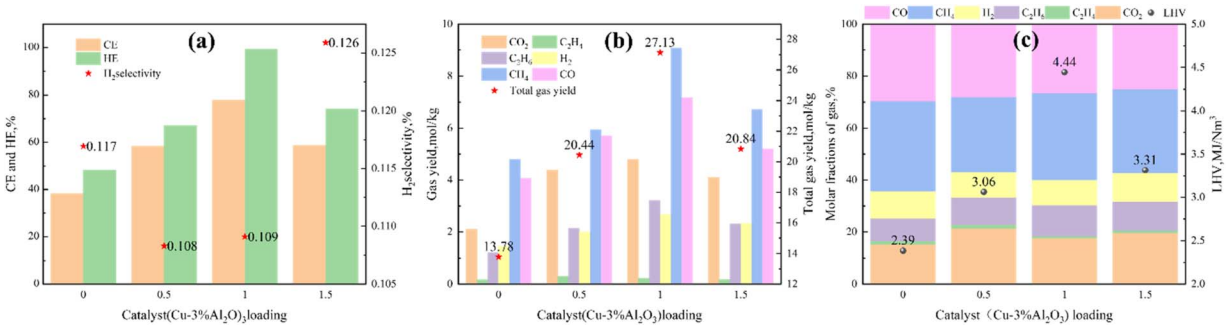

Fig. 6 Influence of Cu-3% Al_2O_3 loading on the supercritical water gasification behavior of wool at 600 °C with a residence time of 5 min and a feedstock concentration of 9 wt% (a) CE, HE, and hydrogen selectivity; (b) gas yields and total gas yield; (c) molar fractions of gas and LHV.

Table 3 Evolution of organic compounds in the liquid phase from wool SCWG

No.	RT/min	Compound name	Peak area percentage/%				
			1 min	3 min	5 min	7 min	9 min
1	5.24	Pyrrole	100	100	58.36	100	100
2	5.44	Toluene	85.01	67.8	100	73.48	99.52
3	8.27	Bicyclo[2.2.1]hept-2-ene, 1-methy	—	11.33	—	—	—
4	8.29	Ethylbenzene	—	—	8.04	2.83	—
5	8.47	1,2-Cyclononadiene	—	4.42	—	—	—
6	8.48	1,3-Cyclopentadiene, 5-(1-methylethylidene)	—	—	4.12	—	—
7	8.49	1,7-Octadiyne	—	—	—	2.83	—
8	11.74	Phenol	—	—	0.7	1.7	7.06
9	14.99	Azulene	—	—	5.13	—	—
10	15	Naphthalene	—	—	—	1.87	—
11	18.49	*m*-Aminophenylacetylene	—	—	—	2.86	—

dehydrogenation and side-chain unsaturation of nitrogen-containing aromatic intermediates under high-temperature conditions.[51,56,57]

Fig. 7 shows the evolution of chromatographic peaks in liquid-phase products as a function of reaction time. At 1–3 min, low-retention-time compounds such as pyrrole and toluene exhibit high peak intensities, which may suggest rapid primary cracking of protein structures and the formation of nitrogen-containing and aromatic intermediates. At 5 min, the increase in aromatic compounds such as ethylbenzene and phenol may indicate the accumulation of secondary liquid-phase intermediates. At 7–9 min, the peak intensities of toluene and pyrrole decrease, while high-retention-time compounds (*e.g.*, naphthalene and *m*-aminophenylacetylene) appear. This trend could suggest further aromatization and condensation of liquid-phase intermediates. In addition, cracking and reforming of aromatic intermediates may occur simultaneously, which could contribute to reduced liquid accumulation and enhanced gasification efficiency.[51,56,57]

Fig. 8 presents a proposed reaction pathway based on the analysis of liquid-phase products obtained during wool SCWG

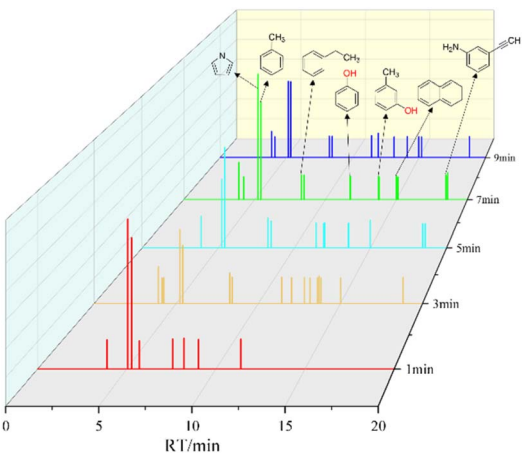

Fig. 7 GC-MS chromatograms of liquid products from wool SCWG at various residence times (600 °C, 9 wt%).

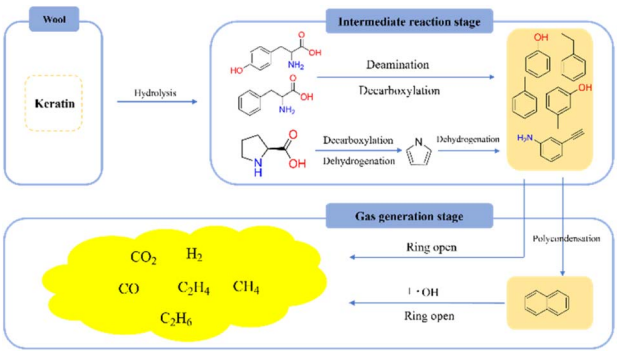

Fig. 8 Reaction pathways of wool SCWG.

at different residence times. It should be noted that this mechanism is inferred from product distribution and should be interpreted as a possible pathway rather than a definitive reaction scheme. The gasification of wool in supercritical water may involve several sequential and parallel steps, including macromolecular depolymerization, aromatization, and secondary cracking reactions. In the initial stage (1 min), keratin may be rapidly hydrolyzed into amino acid intermediates, which could undergo deamination and decarboxylation reactions, leading to the formation of nitrogen-containing heterocycles (*e.g.*, pyrrole) and monocyclic aromatic compounds (*e.g.*, toluene).[51] At intermediate stages (3–5 min), compounds such as ethylbenzene and phenol begin to appear, which may indicate that alkyl rearrangement, dehydrogenation, and partial condensation reactions become more significant, resulting in a more complex mixture of liquid intermediates.[56] At longer residence times (7–9 min), early intermediates may decrease or stabilize, while polycyclic aromatic hydrocarbons (PAHs, such as naphthalene) are formed. This could suggest further aromatization and condensation reactions, leading to the growth of aromatic ring structures. Meanwhile, the decrease in certain liquid intermediates may imply that they are further converted into gaseous products through C–C bond cleavage and possible free radical reactions under supercritical water conditions.[57]

Based on the experimental observations and literature reports, the gasification of wool in supercritical water is likely to involve multiple parallel and consecutive reactions. Initially, wool keratin undergoes hydrolysis and thermal cracking to form smaller intermediates such as amino acids, peptides, oxygenated compounds, and light hydrocarbons. These intermediates may subsequently participate in steam reforming, decarboxylation, methanation, and water–gas shift reactions under supercritical conditions, leading to the formation of H_2, CO, CO_2, CH_4, and light hydrocarbon gases. The final gas composition is therefore considered to result from the dynamic competition between intermediate formation and secondary conversion reactions. In particular, reaction temperature, residence time, feedstock concentration, and catalyst composition may influence the relative contribution of these pathways. It should be noted that the proposed reaction pathways are mainly inferred from product distribution trends and literature reports, while detailed kinetic and mechanistic investigations remain subjects for future study.

2.4. Comparison with previous SCWG studies

Compared with previously reported SCWG studies on protein-rich biomass and other representative feedstocks, the wool feedstock investigated in this study exhibited relatively favorable hydrogen production and gasification performance under supercritical conditions. For example, Su *et al.*[34] reported a hydrogen yield of only 1.74 mol kg^{-1} from food waste at 450 °C and 20 min residence time, while Nanda *et al.*[366] obtained 3.37 mol kg^{-1} H_2 from fructose gasification at 700 °C. In contrast, the maximum H_2 yield obtained from wool SCWG in the present work reached 11.91 mol kg^{-1} under optimal conditions, accompanied by a carbon conversion efficiency of 95.71%, indicating efficient conversion of keratin-derived organic matter into gaseous products.

In addition, the gaseous products from wool SCWG were mainly composed of H_2, CO, CO_2, and CH_4, which is generally consistent with previous SCWG studies on biomass feedstocks. However, compared with conventional biomass systems where CO_2 is usually dominant, relatively higher CO yields were observed in this work. This behavior may be related to the unique keratin structure of wool and the complex decomposition pathways of protein-derived intermediates under supercritical conditions. Overall, the results demonstrate that waste wool exhibits considerable potential as a protein-rich feedstock for hydrogen-rich gas production through SCWG.

3. Conclusions

Waste wool was investigated as a protein-rich feedstock for hydrogen production through supercritical water gasification (SCWG). The effects of reaction temperature, feedstock concentration, residence time, catalyst type, and catalyst loading on gasification behavior and hydrogen production were systematically evaluated in a quartz tubular reactor.

The results showed that increasing temperature significantly promoted gas formation and improved gasification performance. Under the optimal conditions of 600 °C, 2 wt% feedstock concentration, and 5 min residence time, the carbon conversion efficiency (CE) and hydrogen efficiency (HE) reached 95.71% and 119.26%, respectively, with a maximum H_2 yield of 11.91 mol kg^{-1}. The gaseous products were mainly composed of H_2, CO, CO_2, and CH_4.

Among the tested catalysts, Cu-3% Al_2O_3 exhibited the best catalytic performance. Compared with the non-catalytic condition, the catalyst increased CE by 39.63%, HE by 51.13%, and total gas yield by 13.35 mol kg^{-1} under suitable conditions, indicating that Cu-based catalysts can effectively promote the gasification of wool-derived intermediates under supercritical conditions.

Liquid-phase analysis indicated that pyrrole, phenolic compounds, alkylbenzenes, and polycyclic aromatic hydrocarbons were important intermediates during wool SCWG, suggesting that hydrogen production is closely associated with the progressive conversion of keratin-derived organic compounds into gaseous products.

Overall, the results demonstrate that waste wool has considerable potential as a feedstock for hydrogen-rich gas production *via* SCWG. However, detailed catalyst characterization, kinetic analysis, and complete elemental balance analysis were not conducted in the present study. Future work will focus on catalyst structure-performance relationships, nitrogen/sulfur transformation behavior, and more comprehensive thermodynamic and mechanistic investigations.

Author contributions

Wentao Deng: writing – original draft, formal analysis, data curation, conceptualization. Yun Chao: writing – review & editing, project administration, investigation, formal analysis. Qian Li: writing – review & editing, conceptualization, formal analysis, funding acquisition. Bin Chen: supervision, resources, project administration, conceptualization. Zhigang Liu: validation, supervision, resources, project administration. Huiming Chen: resources, methodology, project administration. Lei Yi: validation, supervision, resources. Chuanli Liu: supervision, resources, project administration.

Conflicts of interest

The authors declare no potential conflict of interest regarding this article.

Data availability

The data that support the findings of this study are available from the corresponding author upon reasonable request.

Acknowledgements

This work was supported by Jiangxi Provincial Natural Science Foundation (grant number 20212BAB214027).

Notes and references

1 L. Zhang, C. Jia, F. Bai, W. Wang, S. An, K. Zhao, Z. Li, J. Li and H. Sun, A Comprehensive Review of the Promising Clean Energy Carrier: Hydrogen Production, Transportation, Storage, and Utilization (HPTSU) Technologies, *Fuel*, 2024, **355**, 129455, DOI: 10.1016/j.fuel.2023.129455.

2 M. S. Ng, H. W. B. Teo and A. Chakraborty, Thermodynamic Trends for Evaluating Hydrogen Storage Density and Energy Flow on Maxsorb–III, HKUST–1 and UiO–66 (Zr) MOFs, *Therm. Sci. Eng. Prog.*, 2024, **50**, 102549, DOI: 10.1016/j.tsep.2024.102549.

3 S. Sebastian, S. Wijewardane and S. Srinivasan, Recent Advances in Hydrogen Production, Storage, and Fuel Cell Technologies with an Emphasis on Inventions, Innovations, and Commercialization, *Solar Compass*, 2023, **8**, 100065, DOI: 10.1016/j.solcom.2023.100065.

4 W. Liu, H. Zuo, J. Wang, Q. Xue, B. Ren and F. Yang, The Production and Application of Hydrogen in Steel Industry, *Int. J. Hydrogen Energy*, 2021, **46**, 10548–10569, DOI: 10.1016/j.ijhydene.2020.12.123.

5 D. Prato-Garcia, A. Robayo-Avendaño and R. Vasquez-Medrano, Hydrogen from Natural Gas and Biogas: Building Bridges for a Sustainable Transition to a Green Economy, *Gas Sci. Eng.*, 2023, **111**, 204918, DOI: 10.1016/j.jgsce.2023.204918.

6 W. G. Davies, S. Babamohammadi, Y. Yan, P. T. Clough and S. Masoudi Soltani, Exergy Analysis in Intensification of Sorption–Enhanced Steam Methane Reforming for Clean Hydrogen Production: Comparative Study and Efficiency Optimisation, *Carbon Capture Sci. Technol.*, 2024, **12**, 100202, DOI: 10.1016/j.ccst.2024.100202.

7 R. Al-Farsi and M. Hayyan, Deep Eutectic Solvents: Green Multi–Task Agents for Sustainable Super Green Hydrogen Technologies, *J. Energy Chem.*, 2024, **92**, 357–382, DOI: 10.1016/j.jechem.2023.12.021.

8 B. Çıtmacı, X. Cui, F. Abdullah, D. Richard, D. Peters, Y. Wang, E. Hsu, P. Chheda, C. G. Morales-Guio and P. D. Christofides, Model Predictive Control of an Electrically–Heated Steam Methane Reformer, *Digital Chem. Eng.*, 2024, **10**, 100138, DOI: 10.1016/j.dche.2023.100138.

9 X. Gao, Y. Chen, Y. Wang, L. Zhao, X. Zhao, J. Du, H. Wu and A. Chen, Next–Generation Green Hydrogen: Progress and Perspective from Electricity, Catalyst to Electrolyte in Electrocatalytic Water Splitting, *Nano-Micro Lett.*, 2024, **16**, 237, DOI: 10.1007/s40820-024-01424-2.

10 Z. Sun, Hydrogen Energy: Development Prospects, Current Obstacles and Policy Suggestions under China's "Dual Carbon" Goals, *Chin. J. Urban Environ. Stud.*, 2023, **11**, 2350006, DOI: 10.1142/S2345748123500069.

11 M. Antar, D. Lyu, M. Nazari, A. Shah, X. Zhou and D. L. Smith, Biomass for a Sustainable Bioeconomy: An Overview of World Biomass Production and Utilization, *Renew. Sustain. Energy Rev.*, 2021, **139**, 110691, DOI: 10.1016/j.rser.2020.110691.

12 G. Guan, M. Kaewpanha, X. Hao and A. Abudula, Catalytic Steam Reforming of Biomass Tar: Prospects and Challenges, *Renew. Sustain. Energy Rev.*, 2016, **58**, 450–461, DOI: 10.1016/j.rser.2015.12.316.

13 S. Czernik, R. Evans and R. French, Hydrogen from Biomass–Production by Steam Reforming of Biomass Pyrolysis Oil, *Catal. Today*, 2007, **129**, 265–268, DOI: 10.1016/j.cattod.2006.08.071.

14 Q. Wang, X. Zhang, D. Cui, J. Bai, Z. Wang, F. Xu and Z. Wang, Advances in Supercritical Water Gasification of Lignocellulosic Biomass for Hydrogen Production, *J. Anal. Appl. Pyrolysis*, 2023, **170**, 105934, DOI: 10.1016/j.jaap.2023.105934.

15 J. Zhong, W. Zhu, C. Wang, B. Mu, N. Lin, S. Chen and Z. Li, Transformation Mechanism of Polycyclic Aromatic Hydrocarbons and Hydrogen Production during the Gasification of Coking Sludge in Supercritical Water, *Chemosphere*, 2022, **300**, 134467, DOI: 10.1016/j.chemosphere.2022.134467.

16 R. Coll, J. Salvadó, X. Farriol and D. Montané, Steam Reforming Model Compounds of Biomass Gasification Tars: Conversion at Different Operating Conditions and Tendency towards Coke Formation, *Fuel Process. Technol.*, 2001, **74**, 19–31, DOI: 10.1016/S0378-3820(01)00214-4.

17 M. Mohamadi-Baghmolaei, P. Zahedizadeh, A. Hajizadeh and S. Zendehboudi, Hydrogen Production through Catalytic Supercritical Water Gasification: Energy and Char Formation Assessment, *Energy Convers. Manag.*, 2022, **268**, 115922, DOI: 10.1016/j.enconman.2022.115922.

18 P. Azadi, E. Afif, F. Azadi and R. Farnood, Screening of Nickel Catalysts for Selective Hydrogen Production Using Supercritical Water Gasification of Glucose, *Green Chem.*, 2012, **14**, 1766–1777, DOI: 10.1039/C2GC16378K.

19 Y. Guo, S. Z. Wang, D. H. Xu, Y. M. Gong, H. H. Ma and X. Y. Tang, Review of Catalytic Supercritical Water Gasification for Hydrogen Production from Biomass, *Renew. Sustain. Energy Rev.*, 2010, **14**, 334–343, DOI: 10.1016/j.rser.2009.08.012.

20 Z. Liu, Y. Yang, Y. Chen, L. Yi, L. Guo, Y. Chao and H. Chen, A Review on Catalytic Hydrogen Production from Supercritical Water Gasification of Biomass, *Biomass Bioenergy*, 2024, **190**, 107422, DOI: 10.1016/j.biombioe.2024.107422.

21 Z. Zhang, Z. Ou, C. Qin, J. Ran and C. Wu, Roles of Alkali/Alkaline Earth Metals in Steam Reforming of Biomass Tar for Hydrogen Production over Perovskite Supported Ni Catalysts, *Fuel*, 2019, **257**, 116032, DOI: 10.1016/j.fuel.2019.116032.

22 P. Kuchonthara, B. Puttasawat, P. Piumsomboon, L. Mekasut and T. Vitidsant, Catalytic Steam Reforming of Biomass–Derived Tar for Hydrogen Production with K2CO3/NiO/γ–Al_2O_3 Catalyst, *Korean J. Chem. Eng.*, 2012, **29**, 1525–1530, DOI: 10.1007/s11814-012-0027-y.

23 Y. Luo and J. Chen, Hydrogen Production from Biomass Steam Gasification: Experiment and Simulation, *Chem. Eng. Sci.*, 2024, **292**, 120011, DOI: 10.1016/j.ces.2024.120011.
24 S. N. Reddy, S. Nanda, A. K. Dalai and J. A. Kozinski, Supercritical Water Gasification of Biomass for Hydrogen Production, *Int. J. Hydrogen Energy*, 2014, **39**, 6912–6926, DOI: 10.1016/j.ijhydene.2014.02.125.
25 L. J. Guo, Y. J. Lu, X. M. Zhang, C. M. Ji, Y. Guan and A. X. Pei, Hydrogen Production by Biomass Gasification in Supercritical Water: A Systematic Experimental and Analytical Study, *Catal. Today*, 2007, **129**, 275–286, DOI: 10.1016/j.cattod.2007.05.027.
26 L. Guo, H. Jin and Y. Lu, Supercritical Water Gasification Research and Development in China, *J. Supercrit. Fluids*, 2015, **96**, 144–150, DOI: 10.1016/j.supflu.2014.09.023.
27 Y. Hu, M. Liu, H. Li, X. Han, C. C. Xu and Y. Zeng, Recent Research Progress in Supercritical Water Gasification of Biomass for Hydrogen Production, *Chem. Commun.*, 2025, **61**, 19004–19019, DOI: 10.1039/D5CC05003K.
28 B. Bai, Y. Liu, Q. Wang, J. Zou, H. Zhang, H. Jin and X. Li, Experimental Investigation on Gasification Characteristics of Plastic Wastes in Supercritical Water, *Renew. Energy*, 2019, **135**, 32–40, DOI: 10.1016/j.renene.2018.11.092.
29 S. Nanda, J. Isen, A. K. Dalai and J. A. Kozinski, Gasification of Fruit Wastes and Agro–Food Residues in Supercritical Water, *Energy Convers. Manag.*, 2016, **110**, 296–306, DOI: 10.1016/j.enconman.2015.11.060.
30 Q. Guan, C. Wei and P. E. Savage, Kinetic Model for Supercritical Water Gasification of Algae, *Phys. Chem. Chem. Phys.*, 2012, **14**, 3140–3147, DOI: 10.1039/C2CP23792J.
31 O. Yakaboylu, J. Harinck, K. G. Gerton Smit and W. de Jong, Supercritical Water Gasification of Manure: A Thermodynamic Equilibrium Modeling Approach, *Biomass Bioenergy*, 2013, **59**, 253–263, DOI: 10.1016/j.biombioe.2013.07.011.
32 Y. J. Lu, L. J. Guo, C. M. Ji, X. M. Zhang, X. H. Hao and Q. H. Yan, Hydrogen Production by Biomass Gasification in Supercritical Water: A Parametric Study, *Int. J. Hydrogen Energy*, 2006, **31**, 822–831, DOI: 10.1016/j.ijhydene.2005.08.011.
33 J. A. Okolie, R. Rana, S. Nanda, A. K. Dalai and J. A. Kozinski, Supercritical Water Gasification of Biomass: A State–of–the–Art Review of Process Parameters, Reaction Mechanisms and Catalysis, *Sustain. Energy Fuels*, 2019, **3**, 578–598, DOI: 10.1039/C8SE00565F.
34 W. Su, C. Cai, P. Liu, W. Lin, B. Liang, H. Zhang, Z. Ma, H. Ma, Y. Xing and W. Liu, Supercritical Water Gasification of Food Waste: Effect of Parameters on Hydrogen Production, *Int. J. Hydrogen Energy*, 2020, **45**, 14744–14755, DOI: 10.1016/j.ijhydene.2020.03.190.
35 D. Hantoko, H. Su, M. Yan, E. Kanchanatip, H. Susanto, G. Wang, S. Zhang and Z. Xu, Thermodynamic Study on the Integrated Supercritical Water Gasification with Reforming Process for Hydrogen Production: Effects of Operating Parameters, *Int. J. Hydrogen Energy*, 2018, **43**, 17620–17632, DOI: 10.1016/j.ijhydene.2018.07.198.
36 S. Nanda, S. N. Reddy, H. N. Hunter, A. K. Dalai and J. A. Kozinski, Supercritical Water Gasification of Fructose as a Model Compound for Waste Fruits and Vegetables, *J. Supercrit. Fluids*, 2015, **104**, 112–121, DOI: 10.1016/j.supflu.2015.05.009.
37 A. C. P. Borges, J. A. Onwudili, H. M. C. Andrade, C. T. Alves, A. Ingram, S. A. B. Vieira de Melo and E. A. Torres, Catalytic Supercritical Water Gasification of Eucalyptus Wood Chips in a Batch Reactor, *Fuel*, 2019, **255**, 115804, DOI: 10.1016/j.fuel.2019.115804.
38 J. Huang, C. Zhu, X. Lian, H. Feng, J. Sun, L. Wang and H. Jin, Catalytic Supercritical Water Gasification of Glucose with in–Situ Generated Nickel Nanoparticles for Hydrogen Production, *Int. J. Hydrogen Energy*, 2019, **44**, 21020–21029, DOI: 10.1016/j.ijhydene.2019.04.184.
39 R. Khorasani, M. S. Khodaparasti and O. Tavakoli, Hydrogen Production from Dairy Wastewater Using Catalytic Supercritical Water Gasification: Mechanism and Reaction Pathway, *Int. J. Hydrogen Energy*, 2021, **46**, 22368–22384, DOI: 10.1016/j.ijhydene.2021.04.089.
40 L. Zhang, P. Champagne and C. Xu, Screening of Supported Transition Metal Catalysts for Hydrogen Production from Glucose via Catalytic Supercritical Water Gasification, *Int. J. Hydrogen Energy*, 2011, **36**, 9591–9601, DOI: 10.1016/j.ijhydene.2011.05.077.
41 S. Nanda, A. K. Dalai, I. Gökalp and J. A. Kozinski, Valorization of Horse Manure through Catalytic Supercritical Water Gasification, *Waste Manag.*, 2016, **52**, 147–158, DOI: 10.1016/j.wasman.2016.03.049.
42 Li. Haoyang, Z. Mingyuan, W. Haoyu, H. Xue, Z. Yimin and C. C. Xu, Comparison study of supercritical water gasification for hydrogen production on a continuous flow versus a batch reactor, *Bioresour. Technol.*, 2024, **391**, 129923, DOI: 10.1016/j.biortech.2023.129923.
43 F. Camilli, M. Focacci, A. Dal Prà, S. Bortolu, F. Ugolini, E. Vagnoni and P. Duce, Turning Waste Wool into a Circular Resource: A Review of Eco–Innovative Applications in Agriculture, *Agronomy*, 2025, **15**, 446, DOI: 10.3390/agronomy15020446.
44 B. Xu, Q. Chen, B. Fu, R. Zheng and J. Fan, Current Situation and Construction of Recycling System in China for Post–Consumer Textile Waste, *Sustainability*, 2022, **14**, 16635, DOI: 10.3390/su142416635.
45 B. Mu, X. Yu and Y. Yang, Sustainable and Green Process for Recycling Waste Wool Textiles into High–Quality Protein Fibers on a Pilot Scale, *Resour. Conserv. Recycl.*, 2023, **198**, 107190, DOI: 10.1016/j.resconrec.2023.107190.
46 M. Shamsuzzaman, M. Islam, Md. A. Al. Mamun, R. Rayyaan, K. Sowrov, S. Islam and A. S. M. Sayem, Fashion and Textile Waste Management in the Circular Economy: A Systematic Review, *Cleaner Waste Syst.*, 2025, **11**, 100268, DOI: 10.1016/j.clwas.2025.100268.
47 J. Bradbury and G. Chapman, The Chemical Composition of Wool, *Aust. J. Biol. Sci.*, 1964, **17**, 960–972, DOI: 10.1071/BI9640960.
48 F. Sabatini, T. Nacci and I. Degano, Colombini. Investigating the composition and degradation of wool through EGA/MS

and Py–GC/MS, *J. Anal. Appl. Pyrolysis*, 2018, **135**, 111–121, DOI: 10.1016/j.jaap.2018.09.012.

49 Y. Nancy, D. P. Acelas, D. W. F. López, W. Brilman, S. R. A. Kersten and A. M. J. Kootstra, Supercritical water gasification of sewage sludge: Gas production and phosphorus recovery, *Bioresour. Technol.*, 2014, **174**, 167–175, DOI: 10.1016/j.biortech.2014.10.003.

50 K. Heeley, R. L. Orozco, L. E. Macaskie, J. Love and B. Al-Dur, Supercritical water gasification of microalgal biomass for hydrogen production-A review, *Int. J. Hydrogen Energy*, 2024, **49**, 310–336, DOI: 10.1016/j.ijhydene.2023.08.081.

51 R. Dong, H. Jia, J. Tian, Z. Liu, Z. Peng, J. Xu, H. Jin, B. Chen and L. Guo, Food Waste Supercritical Water Gasification for Combustible Gas Production: Product Distribution, Conversion Pathways, Kinetic Characteristics, *Renew. Energy*, 2026, **256**, 124473, DOI: 10.1016/j.renene.2025.124473.

52 Z. Peng, S. Rong, J. Xu, H. Jin, J. Zhang, F. Shang and L. Guo, Reaction Pathways and Kinetics for Hydrogen Production by Oilfield Wastewater Gasification in Supercritical Water, *Fuel*, 2026, **314**, 123135, DOI: 10.1016/j.fuel.2022.123135.

53 Y. Qiu, Z. Huang, L. Yi, B. Chen and B. Chen, Investigation of Bamboo Gasification Behavior in Supercritical Water and Hydrogen Production, *Biomass Bioenergy*, 2025, **202**, 108185, DOI: 10.1016/j.biombioe.2025.108185.

54 Y. Chen, Y. Ma, C. Liao, J. You, H. Fang, C. Chen, Y. Luo and L. Jiang, A Confinement-Stabilized Cu0–Cu+ Redox Pair on Silica and Its Catalytic Role in the Water–Gas Shift Reaction, *J. Mater. Chem. A*, 2025, **13**, 29079–29091, DOI: 10.1039/D5TA03435C.

55 C. Huang, Y. Chen, H. Fang, G. Zhi, C. Chen, Y. Luo, X. Lin and L. Jiang, Copper Phyllosilicate-Derived Cu Catalyst for the Water–Gas Shift Reaction: Insight into the Role of Cu+–Cu0 and Reaction Mechanism, *ACS Catal.*, 2025, **15**, 5546–5556, DOI: 10.1021/acscatal.4c07785.

56 W. Cui, J. Hui, F. Huifang, W. Wenwen, C. Changqing and C. Wen, Study on gasification mechanism of biomass waste in supercritical water based on product distribution, *Int. J. Hydrogen Energy*, 2020, **45**, 28051–28061, DOI: 10.1016/j.ijhydene.2020.02.146.

57 W. Cui, Z. Chao, H. Jianbing, H. Jin. and X. Lian, Gasification of biomass model compounds in supercritical water: Detailed reaction pathways and mechanisms, *Int. J. Hydrogen Energy*, 2022, **45**, 31843–31851, DOI: 10.1016/j.ijhydene.2021.12.008.